Eur Biophys J (1985) 13:77–88

European Biophysics Journal

A comparison of the structure and dynamics of avian pancreatic polypeptide hormone in solution and in the crystal

P. Krüger[1], W. Straßburger[1*], A. Wollmer[1], and W. F. van Gunsteren[2]

[1] Lehr- und Forschungsgebiet Struktur und Funktion der Proteine, Abteilung Physiologische Chemie, Rheinisch-Westfälische Technische Hochschule Aachen, Klinikum Pauwelsstrasse, D-5100 Aachen, Federal Republic of Germany
[2] Laboratory of Physical Chemistry, The University of Groningen, Nijenborgh 16, NL-9747 AG Groningen, The Netherlands

Received March 8, 1985 / Accepted in revised form July 8, 1985

Abstract. A molecular dynamics simulation was carried out with avian pancreatic polypeptide hormone (aPP) as an isolated monomer explicitly including the solvent (MDS). The simulation and the resulting mean structure are compared with the results of a corresponding crystal simulation (MDC) with 4 aPP molecules plus interstitial water in a periodic boundary unit cell and with the X-ray structure (van Gunsteren, Haneef et al., manuscript in preparation). Comparison is based on the time span 5 to 15 ps and considering cartesian coordinates, dihedral angles, H-bond length, and accessible surface area. While in the MDC simulation equilibration is fast and complete, it does occur in MDS for most but not all parts of the molecule; the turn region starts moving away from the X-ray structure after 9 ps.

Only minor differences result when dimer-forming side chains, e.g. tyrosines 7 and 21, are exposed to solvent. The largest rms fluctuations are encountered in exposed polar side chains of Asp 11, Glu 15, Arg 19, and Arg 33, but also in the hydrophobic core residue Phe 20, the only phenylalanine residue present. The latter undergoes an abrupt reorientation suitable for verification by NMR spectroscopy, which is possibly related to the motion of the turn region. The main-chain dihedral angles of the α-helix are shifted from values generally found in crystal structures towards those of the ideal Pauling helix. There is concomitant H-bond elongation. The effects are most pronounced and consistent in the MDS simulation.

Abbreviations: MD, molecular dynamics; MDS, molecular dynamics simulation in solution; MDC, same in the crystal; $\overline{\text{MDS}}$, mean structure obtained by averaging the transient atomic coordinates over 5–15 ps of the solvent simulation; $\overline{\text{MDC}}$, same of the crystal simulation; X, X-ray structure; GROMOS, Groningen Molecular Simulation System; CD, circular dichroism; aPP, avian pancreatic polypeptide hormone; one and three-letter abbreviations for amino acids are used.

Key words: Molecular dynamics, avian pancreatic polypeptide, solvent, comparison with crystal

1. Introduction

The only molecular dynamics simulation of a protein in which the solvent environment has been explicitly taken into account so far is that of pancreatic trypsin inhibitor (van Gunsteren and Karplus 1982; van Gunsteren et al. 1983; van Gunsteren and Berendsen 1984). Avian pancreatic polypeptide hormone is another molecule which because of its size and the accuracy of its X-ray structure (Blundell et al. 1981; Glover et al. 1983) seems suitable for this approach. Though consisting of no more than 36 amino acids and lacking disulphide bridges it has a surprisingly stable structure and could be thought of as the quintessence of a globular protein. With almost all residues organized in two roughly antiparallel helices it is hardly more than a folding unit. Prolines in positions 2, 5 and 8 (for the amino acid sequence see Fig. 7) induce a left-handed polyproline II helix extending from positions 1 to 8. A type I β-bend between positions 9 and 12 is followed by a good α-helix from position 14 to 31 whereas the remaining 5 C-terminal residues are conformationally less defined. The packing together of the helices with their non-polar faces together gives the molecule a hydrophobic core. Further surface non-polar groups on the α-helix but also ionizable groups with pK ≅ 5 are responsible for entropically driven formation of a very stable symmetrical dimer ($K_{12} \cong 3 \cdot 10^7 M^{-1}$) which also exists in the crystal. CD spectroscopic studies indicated that the main-chain conformation is also stable when aPP exists as a monomer in solution (Glover et al. 1984).

Besides the fact that a broader basis of experience for the young technique of molecular dynamics simulation is desirable a study of aPP promises

specific contributions: In contrast to pancreatic trypsin inhibitor its structure 1) is not braced by disulphide bonds, 2) allows one to analyze motions within two different types of well developed helices as well as 3) of the helices relative to one another and 4) lends itself to identifying mutual influences of the monomers within a dimer.

Two simulations have been carried out for the structure and dynamics of aPP: The one, designated MDC, is for aPP in its environment in the crystal (van Gunsteren, Haneef et al. in preparation), the other, MDS, for an aPP monomer in solution. The monomer was chosen deliberately because it is believed to be the biologically active species and the behaviour of residues exposed to solvent upon separation of the dimer is of particular interest. Regrettably the computing time available did not allow for a simulation longer than 15 ps.

In this communication the mean structures generated in the two simulations are compared with respect to parameters such as cartesian coordinates, dihedral angles, H-bonds, and accessible surface area while the mean structure from the crystal run is mainly compared to the X-ray structure. Comparison of two simulated structures will minimize the risks of possible artefacts originating in the limited adequacy of the energy potentials used. A more detailed analysis of the solvent simulation with respect to frequencies and correlations of motions will be dealt with in a subsequent publication.

2. Model and computational procedure

The programs for performing and analyzing the simulations were taken from the GROMOS library (van Gunsteren). The energy potential function used is of the type that is generally applied to proteins (van Gunsteren and Berendsen 1982). Hydrogen atoms attached to carbon atoms are incorporated into the latter, whereas the other hydrogen atoms capable of hydrogen bond formation are explicitly treated. Bond lengths were kept constant by means of the SHAKE method (van Gunsteren and Berendsen 1977). Non-bonded interactions were taken into account only within a cut-off radius of $R_c = 8$ Å. The values of non-bonded interaction parameters and the partial atomic charges have been given by Hermans et al. (1984). The water molecules were modelled by a simple rigid three-point charge model (SPC model, Berendsen et al. 1981) which has been specially developed for use in mixed protein/water systems and which adequately describes the properties of bulk water at ordinary temperatures. Periodic boundary conditions were applied to both the MDC and MDS simulation. The initial velocities were taken from a Maxwell distribution. 300 K was the initial temperature and also that of a temperature bath the system was coupled to using the method described by Berendsen et al. (1984) and a coupling relaxation time $\tau = 0.1$ ps. The time step for integration of the equation of motion was 0.002 ps. The MDC and MDS simulations were carried over 15 ps. Analyses (e.g. calculation of mean structure, rms fluctuations etc.), however, were mostly based on the last 10 ps. Transient structures were analyzed with the help of specially developed graphics programs (Straßburger unpublished).

APP crystallizes with zinc ions in space group C2 (Blundell et al. 1981). The dimensions of the unit cell are $a = 34.18$ Å; $b = 32.92$ Å; $c = 29.44$ Å; $\beta = 105.3°$. It contains one dimer plus two half dimers. Accordingly the MDC simulation refers to 4 monomers in a box with 388 molecules of interstitial water. Molecule 3 was arbitrarily selected for comparison with the monomer of the MDS simulation. The water molecules were distributed statistically in the space between the aPP molecules without reference to the crystallographically determined water positions. One aPP molecule consists of 370 atoms including 1 zinc ion which was left out in the MDS simulation. For this simulation a single molecule was placed in a box of $a = 24.47$ Å; $b = 30.58$ Å; $c = 46.88$ Å and $\beta = 90°$ in such a way that its minimum distance from any wall of the box was $\geqq 3.5$ Å. In this arrangement, as has been checked for the starting geometry, any atoms of different aPP molecules related by the periodic boundary conditions are separated by more than the cut-off radius of 8 Å. The space around the polypeptide accommodated 1022 water molecules. During energy minimization both the protein and the solvent were allowed to relax simultaneously. When simulating even a small protein in solution, a compromise has to be found between the size of the system (i.e. the number of solvating water molecules) and the length of the molecular dynamics run on the one hand and the available computer power on the other. Because of the time consuming character of protein simulations only two simulations (of 20 ps length) of a protein – bovine pancreatic trypsin inhibitor – in water have been published (van Gunsteren and Karplus 1982; van Gunsteren and Berendsen 1984).

3. Results and discussion

Time course

The potential energy in the course of the solvent run is depicted in Fig. 1. The high initial energy is due

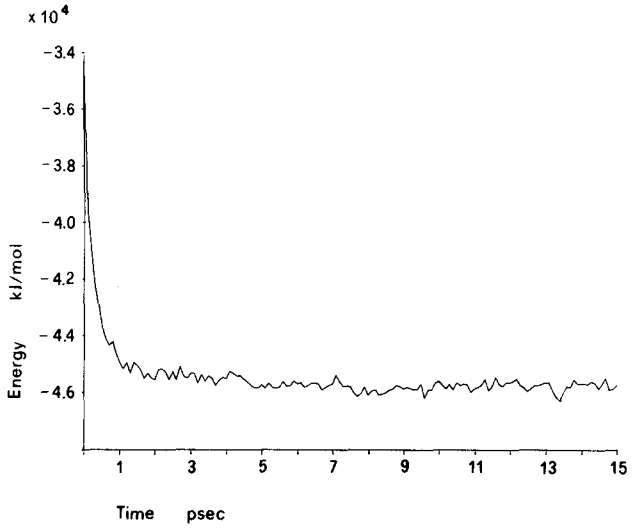

Fig. 1. Potential energy in the course of the solvent simulation, MDS

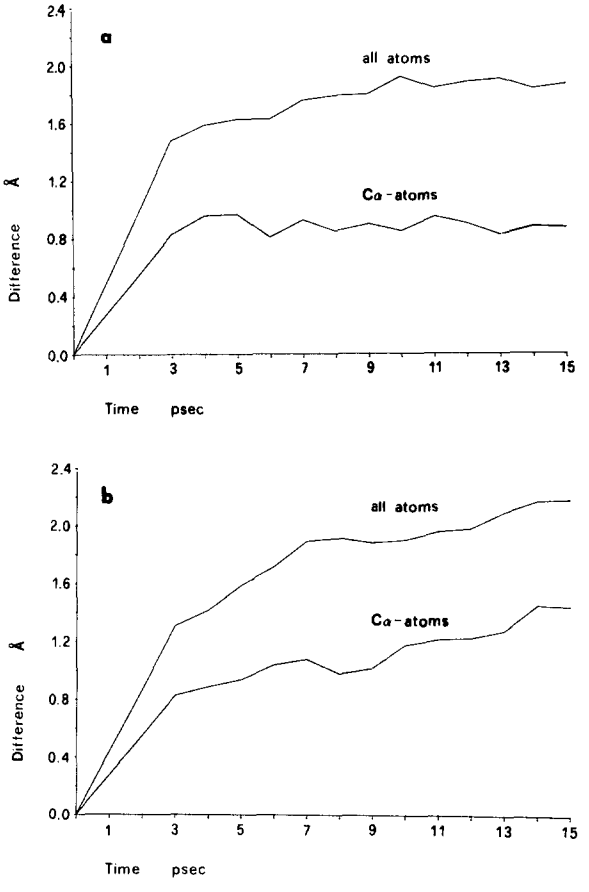

Fig. 2. Rms positional differences as a function of simulation time. **a** MDC simulation; **b** MDS simulation

to the fact that the water molecules were randomly placed in the empty space surrounding the protein. It is quickly reduced within the first ps, levels off after 4 ps and from then on oscillates about an average value of 45,700 kJ/mol. The development of the

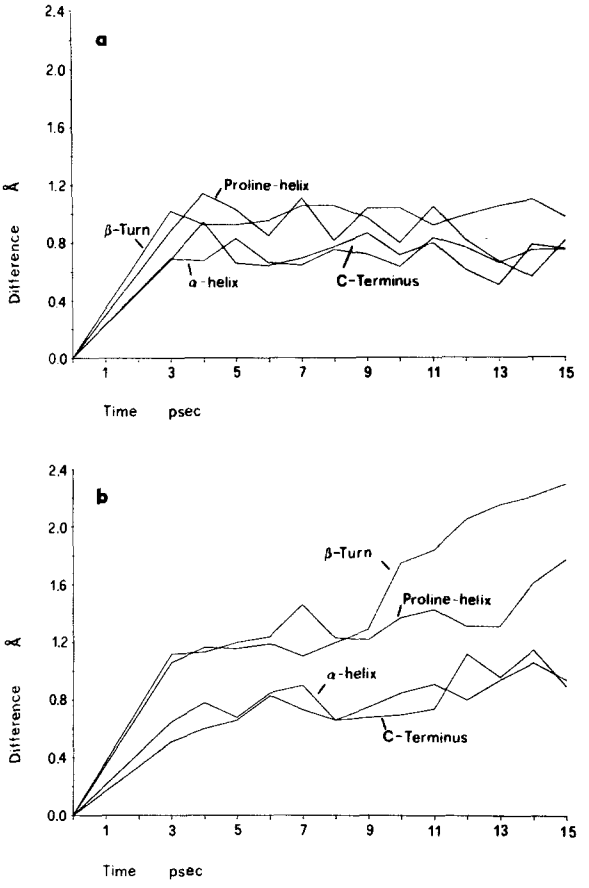

Fig. 3. Rms positional differences as a function of simulation time. Averages were calculated for each conformational segment separately, including main and side-chain atoms. **a** MDC simulation; **b** MDS simulation

rms positional differences from the X-ray structure ($t = 0$) for the MDC and the MDS simulation is shown in Fig. 2. The major part of the drift away from the X-ray structure is related to the fall of the potential energy during the first 3 ps. After 5 ps 88% of the maximum drift in the MDC and 76% of that in the MDS simulation has occurred. For the solvent run the unidirectional trend in the deviations still occurring between 5 and 15 ps (MDS, Fig. 2b) indicates that at the end of the simulation equilibrium might not have been fully attained. Irrespective of this concern the comparison of MDS and MDC described below seems justified and valuable.

The rms positional differences as a function of time plotted in Fig. 3 were calculated separately for the C_α atoms in each of the constituent conformational segments of aPP. In the crystal run the polyproline (residues 1–8), β-turn (9–12), α-helical (14–31), and C-terminal (32–36) segments all exhibit values fluctuating about a constant level, a behaviour reflecting the reliability of the approach. In the solvent run this pattern is shared by all segments except one: After 9 ps the β-turn region starts

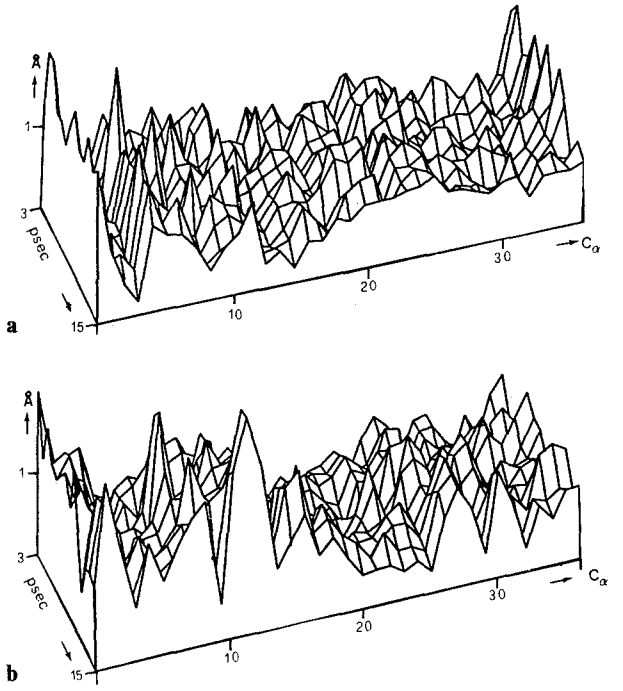

Fig. 4. Rms positional differences of C_α atoms as a function of simulation time (at 1 ps intervals) and sequence position. **a** MDC simulation; **b** MDS simulation

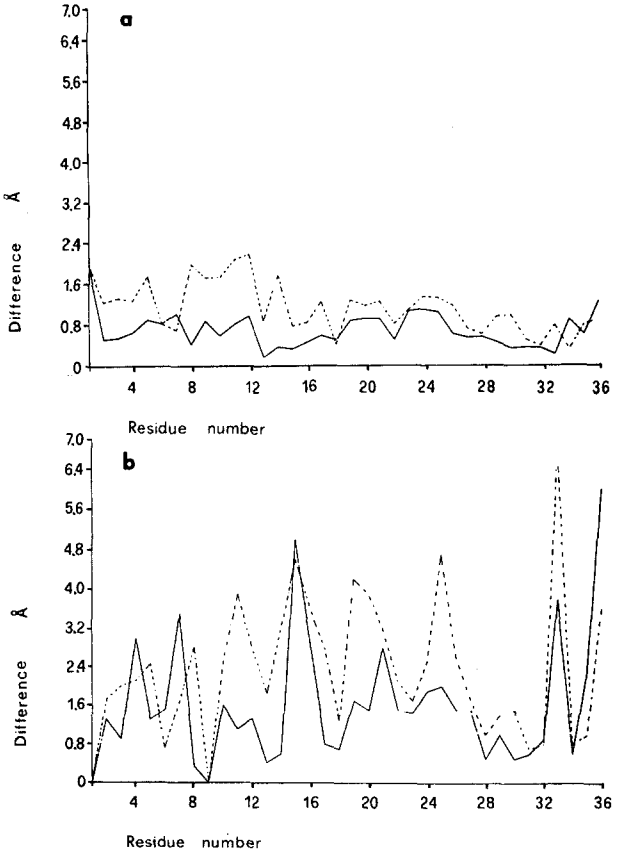

Fig. 5. Rms positional differences between X-ray structure and $\overline{\text{MDC}}$ (*full lines*) and between $\overline{\text{MDS}}$ and $\overline{\text{MDC}}$ (*dotted lines*). **a** averages over C_α atoms; **b** averages over outermost side-chain atoms

moving away from its position in the X-ray structure and also affects the polyproline helix. Figure 4, for which the values were calculated individually for each C_α atom, clearly shows that the residues of the polyproline helix most affected by the movement are those next to the turn.

Comparison of structures

Cartesian coordinates. For structural comparison the transient atomic coordinates from 5 to 15 ps of a simulation were averaged. The mean structure of the solvent simulation ($\overline{\text{MDS}}$) is compared with that of the crystal simulation ($\overline{\text{MDC}}$) whereas the latter is compared with the X-ray structure (X). As a preliminary step two structures to be compared are superimposed by a least squares fit. The distances then remaining between corresponding atoms are represented for C_α atoms in Fig. 5a and for the outermost side-chain atoms in Fig. 5b. These remaining distances were averaged over the whole sequence and listed in Table 1. The smallest values are found for C_α atoms which are positionally more conservative than side-chain atoms. In general the remaining differences are considerably larger for $\overline{\text{MDC}}$-$\overline{\text{MDS}}$ than for X-$\overline{\text{MDC}}$. However, calculation of X-$\overline{\text{MDS}}$ shows that $\overline{\text{MDS}}$ is not much farther away from the X-ray structure than is $\overline{\text{MDC}}$.

If the remaining differences are considered with respect to sequence position a uniform distribution is encountered for C_α atoms with X-$\overline{\text{MDC}}$ (Fig. 5a, full line). Those with $\overline{\text{MDC}}$-$\overline{\text{MDS}}$ typically exhibit an accumulation of above-average values in the turn region (Fig. 5a, dotted line). This, of course, is a reflexion of the turn drift discovered above in the analysis of the time course of the MDS simulation (Figs. 3b and 4b). The phenomenon is blurred in Fig. 5b because of the larger distances generally remaining between outermost side-chain atoms (see Table 1 for averages). The largest remaining differences between individual residues are those encountered with the exposed hydrophilic side chains of Glu 15, Arg 33, and Tyr 36 in X-$\overline{\text{MDC}}$ and Asp 11, Arg 19, Gln 25, and Arg 33 and $\overline{\text{MDC}}$-$\overline{\text{MDS}}$. Of

Table 1. Average distances between corresponding atoms remaining after optimum superposition of $\overline{\text{MDC}}$, $\overline{\text{MDS}}$, and the X-ray structure

Average over	X-$\overline{\text{MDC}}$ [Å]	X-$\overline{\text{MDS}}$ [Å]	$\overline{\text{MDC}}$-$\overline{\text{MDS}}$ [Å]
C_α atoms	0.79	1.05	1.24
side-chain atoms	1.47	1.87	2.08
outermost side-chain atoms	1.72	2.36	2.47
all atoms	1.64	1.80	2.16

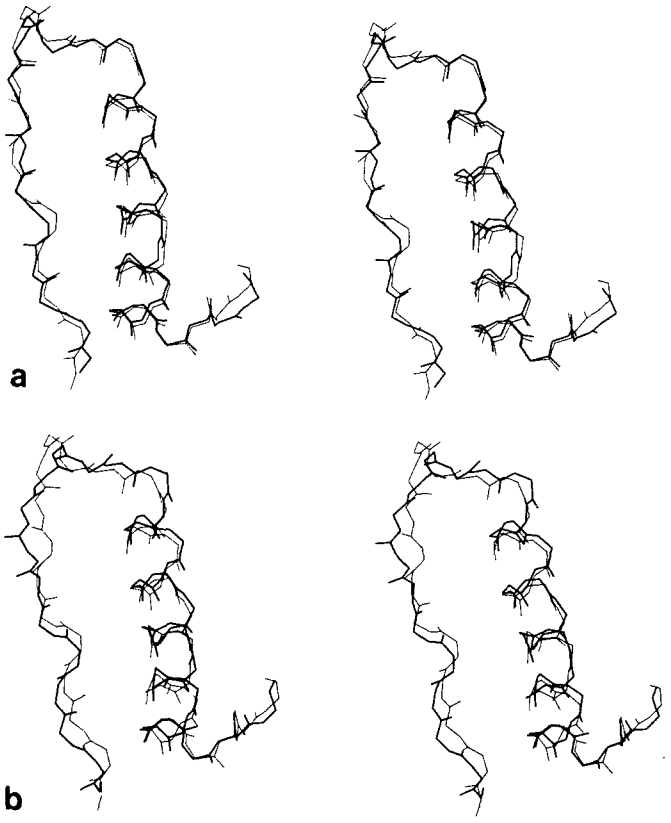

Fig. 6. Stereopairs of the backbone structures fitted to optimum superposition. **a** of the X-ray structure (——) and $\overline{\text{MDC}}$ (——) and **b** of $\overline{\text{MDS}}$ (——) and $\overline{\text{MDC}}$ (——)

Table 2. Absolute differences in dihedral angles of the mean simulated structures $\overline{\text{MDC}}$ and $\overline{\text{MDS}}$ and the X-ray structure

Angles averaged	*X*-$\overline{\text{MDC}}$	*X*-$\overline{\text{MDS}}$	$\overline{\text{MDC}}$-$\overline{\text{MDS}}$
φ	19.0°	22.4°	27.1°
ψ	20.1°	34.8°	40.3°
χ^1	39.0°	45.3°	45.5°
all	33.0°	42.1°	43.4°

these the residues Asp 11, Gln 25, and Arg 33 are involved in hydrogen bonds to adjacent aPP molecules in the crystal, whereas the side chains of Glu 15, Arg 19, and Tyr 36 are hydrogen bonded to crystalline water molecules. Changing the crystalline environment for that of an aqueous solution may easily change the average positions of these polar side chains. Side chains involved in contacts between monomers in the dimer, such as Tyr 7 or Tyr 21, do not impose significantly larger differences in $\overline{\text{MDC}}$-$\overline{\text{MDS}}$.

Since absolute positional differences do not carry any information on their spatial distribution the structures fitted to optimum superposition are depicted as stereopairs in Fig. 6 for direct comparison by inspection.

Dihedral angles. All dihedral angles of $\overline{\text{MDC}}$ and $\overline{\text{MDS}}$ were calculated. For comparison of two structures the absolute differences of corresponding dihedral angles were calculated and averaged again, in certain groupings, this time over the sequence. The sequence averages of the differences in dihedral angles between $\overline{\text{MDS}}$, $\overline{\text{MDC}}$ and X-ray structures are listed in Table 2. Larger deviations in dihedral angles are found between $\overline{\text{MDC}}$ and $\overline{\text{MDS}}$ than between $\overline{\text{MDC}}$ and the X-ray structure. However, as in the case of the positional differences (Table 1) these are more pronounced than the deviations of each of the mean simulated structures from the X-ray structure.

For the individual φ/ψ pairs of main chain dihedral angles the signed differences are plotted along the aPP backbone as a histogram in Fig. 7. Several of the more substantial differences are conformationally more or less inconsequential because of the compensatory effect of opposite differences in the adjacent angle of the preceding or following residue. This applies to ψ_8/φ_9 and ψ_{11}/φ_{12} in *X*-$\overline{\text{MDC}}$ (Fig. 7a) and to ψ_9/φ_{10}, φ_{11}/ψ_{12}, ψ_{16}/φ_{17}, ψ_{33}/φ_{34}, and ψ_{35}/φ_{36} im $\overline{\text{MDC}}$-$\overline{\text{MDS}}$ (Fig. 7b). Uncompensated differences are found in *X*-$\overline{\text{MDC}}$ for ψ_5, φ_{18}, and ψ_{35}, and in $\overline{\text{MDC}}$-$\overline{\text{MDS}}$ for ψ_{10}, φ_{18}, and ψ_{32}. It appears noteworthy that in the two helices the angular changes obtained in the $\overline{\text{MDC}}$-$\overline{\text{MDS}}$ comparison are not as pronounced as those in the *X*-$\overline{\text{MDC}}$ comparison. Constancy of dihedral angles in combination with elevated positional differences, as encountered for the polyproline helix (compare Figs. 5b and 7b), may indicate that a structural segment undergoes a mainly translatory shift. The ψ_{10} and the uncompensated portion of the ψ_{11} differences between $\overline{\text{MDS}}$ and $\overline{\text{MDC}}$ are an expression of the turn motion in the solvent run. The largest absolute differences (> 140°) of all are encountered with side-chain dihedral angles of Arg 19 and Arg 33 in both *X*-$\overline{\text{MDC}}$ and $\overline{\text{MDC}}$-$\overline{\text{MDS}}$.

Hydrogen bonds. The mean simulated structures, $\overline{\text{MDC}}$ and $\overline{\text{MDS}}$, and the X-ray structure were further compared with respect to hydrogen bonds. An H-bond was decided to exist if the donor-acceptor distance was < 3.3 Å and the donor-H-acceptor bond angle > 135°. The intramolecular H-bonds identified in any of the three structures are listed in Table 3. Those in the turn region involving residues 9, 12, and 13 are lost in $\overline{\text{MDS}}$ but also in $\overline{\text{MDC}}$ which does not include the special turn motion described above. The mean simulated struc-

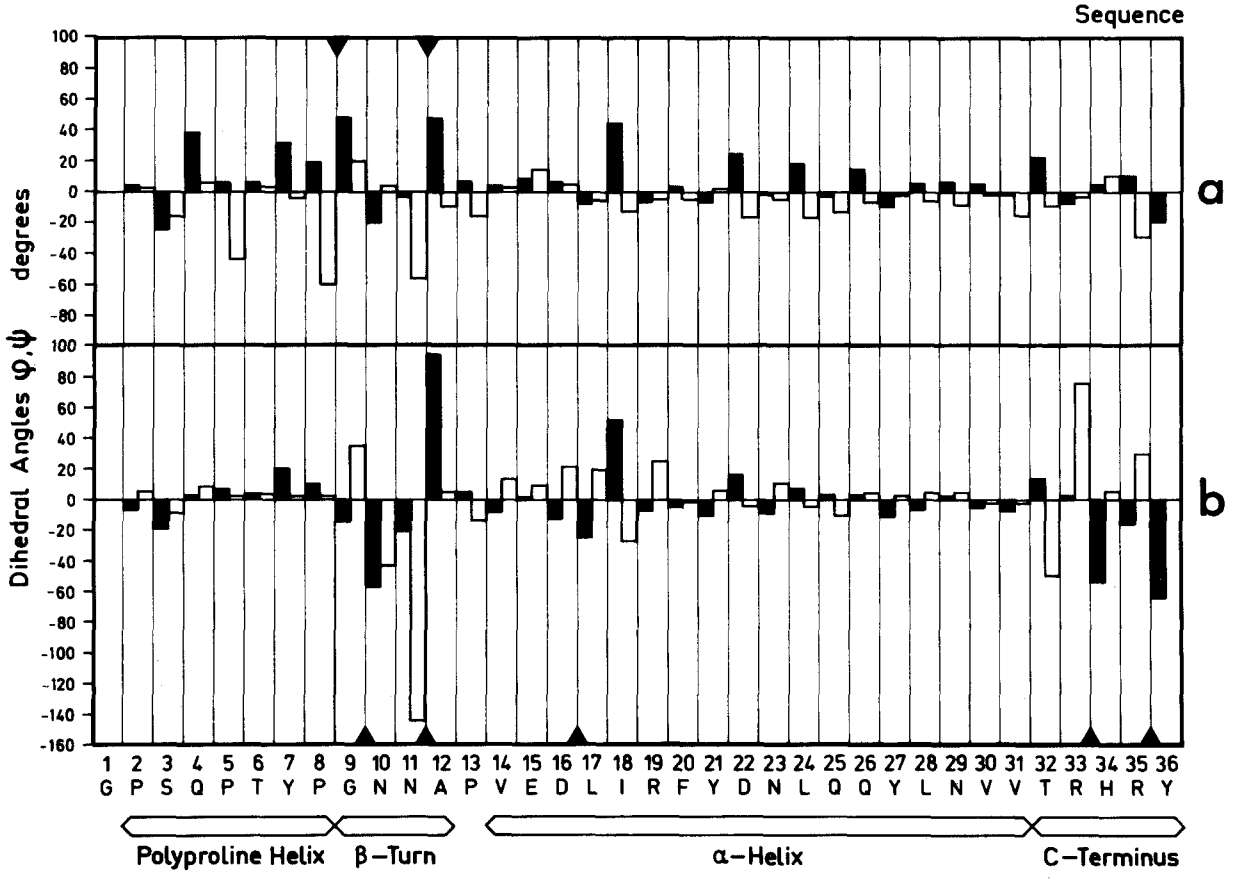

Fig. 7. Differences in the pairs of main-chain dihedral angles φ (*full columns*) and ψ (*open columns*). **a** between X-ray structure and $\overline{\text{MDC}}$ and **b** between $\overline{\text{MDS}}$ and $\overline{\text{MDC}}$. ▲ indicates positions where conformational consequences are reduced due to opposite differences in the ψ and φ angles of adjacent residues

Table 3. Intramolecular hydrogen bonds identified in the $\overline{\text{MDC}}$, $\overline{\text{MDS}}$ and X-ray structure of aPP

Donor	Acceptor	X-ray	$\overline{\text{MDC}}$	$\overline{\text{MDS}}$
12 Ala N	9 Gly O	+	–	–
16 Asp N	13 Pro O	+	–	–
17 Leu N	13 Pro O	+	+	+
18 Ile N	14 Val O	+	+	+
19 Arg N	15 Glu O	+	–	+
20 Phe N	16 Asp O	+	+	+
21 Tyr N	17 Leu O	+	+	+
22 Asp N	18 Ile O	+	+	+
23 Asn N	19 Arg O	+	+	+
24 Leu N	20 Phe O	+	+	+
25 Gln N	21 Tyr O	+	+	+
26 Gln N	22 Asp O	+	+	+
27 Tyr N	23 Asn O	+	+	+
28 Leu N	24 Leu O	+	+	+
29 Asn N	25 Gln O	+	+	+
30 Val N	26 Gln O	+	+	+
31 Val N	27 Tyr O	+	+	+
32 Tyr N	28 Leu O	+	+	+
33 Arg N	30 Val O	+	–	–
33 Arg N	31 Val O	–	+	+
34 His N	29 Asn O	+	–	–
34 His N	32 Thr O	–	+	+
7 Tyr O^{η}	10 Asp O^{δ_2}	+	+	+

tures both offer acceptor alternatives for the imido protons of Arg 33 and His 34 which in the X-ray structure are engaged with carbonyls 29 and 30 at the end of the α-helix.

For the solvent run H-bonds were also identified between the backbone of transient simulated aPP structures and molecules of the surrounding water. (Since averaging is not straightforward here, this is not readily feasible in the case of mean simulated structures). There are two carbonyls, those of Pro 2 and Ser 3, which at the end of the simulation still bind the same water molecules they bound after 5 ps. While water exchange seems to be normal at most backbone acceptors some, e.g. Leu 17 and Ile 18, tend not to have water within H-bond distance. The interaction of aPP with the surrounding water will be dealt with in more detail in another paper.

Accessible surface area. The surface area of aPP accessible for solvent molecules was calculated with the algorithm introduced by Lee and Richards 1971 with 1.6 Å for the radius of water (Pearlman 1981).

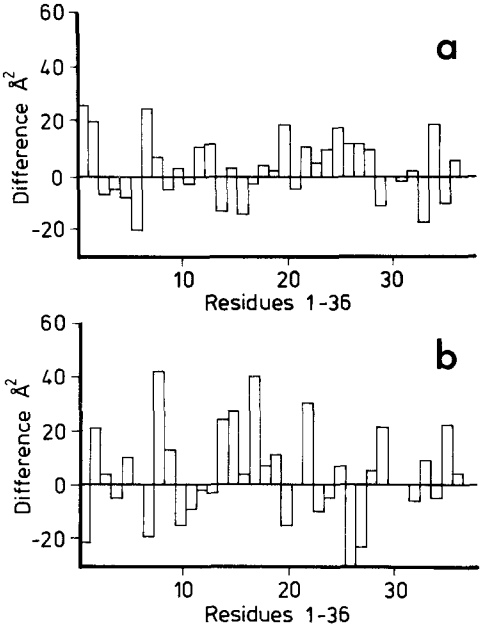

Fig. 8. Differences in solvent-accessible surface area between **a** MDC and the X-ray structure; **b** MDS and MDC. (Differences due to contacts between monomers have been eliminated)

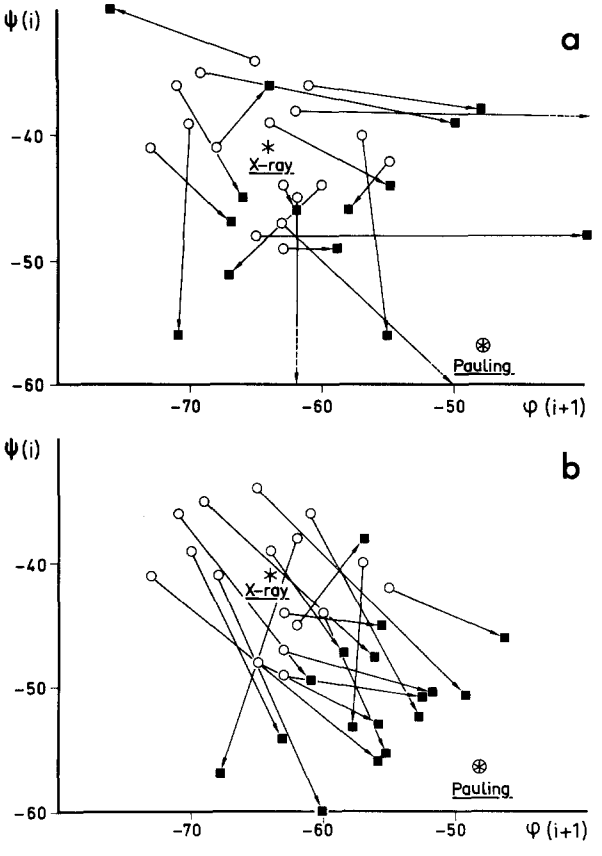

Fig. 9. Main-chain dihedral angles ψ_i and φ_{i+1} of the α helix (residues $i = 14-31$) in aPP. **a** X-ray structure ○ and MDC ■; **b** X-ray structure ○ and MDS ■

The calculations were carried out for MDC, MDS, and the X-ray structure and are referring to a monomer throughout, i.e. any quaternary structural shielding against the solvent in MDC and the X-ray structure was ignored. Figure 8 shows the differences in accessible surface area for *X* and MDC (a) and MDC and MDS (b). In MDC notably Gly 1 and Tyr 7 are more exposed than in the X-ray structure, however, there are also residues which are rather more buried, Thr 6 and Arg 33 for example. There is a moderate increase in accessible surface area of 4%. Several of the differences between X-ray and MDC are still further increased when going from MDC to MDS. This observation applies to Pro 2, Pro 8, Glu 15, Leu 17, and Asp 22. In total the accessible surface area of MDS exceeds that of MDC by 5%. No significant differences can be seen in the behaviour of hydrophilic or hydrophobic residues or residues involved or not involved in dimer formation. Tyr 7 and Tyr 21, for instance, which are exposed upon dissociation of the dimer, do not avoid solvent contact, possibly due to their side-chain hydroxyl.

α-helix. The several structural parameters considered above are now used synoptically for a more detailed comparison restricted to the α-helical segment. Table 4 reflects a clear tendency of the simulations to shift the main-chain dihedral angles from the average values normally encountered with helices in protein X-ray structures (Blundell et al. 1983) towards those of the ideal Pauling helix. This tendency is more pronounced for the MDS than for the MDC simulation and, as illustrated by Fig. 9, much more systematic. According to Blundell et al. (1983) the values for helices in protein crystals are an outcome of unbalanced interaction with solvent due to the amphipathic nature of the helices, which also causes their curvature through an increase in length of water-exposed H-bonds. The H-bond lengths for the α-helix of aPP are listed in Table 5. For the X-ray structure the longest H-bonds are typically found in polar environments. In MDC

Table 4. Average main-chain dihedral angles of the α-helix (residues 14–31) in MDC, MDS and the X-ray structure of aPP

Structure		φ	ψ
X-ray	general	−63°	−43°
	aPP_{14-31}	−64°	−41°
	MDC_{14-31}	−57°	−48°
	MDS_{14-31}	−55°	−51°
Pauling		−48°	−57°

Table 5. Length of the hydrogen bonds in the α-helix of aPP (residues 14–31)

Donnor-acceptor pair (N–O)	Donor-acceptor distance [Å]		
	X-ray	$\overline{\text{MDC}}$	$\overline{\text{MDS}}$
14–18	2.86	2.78	3.19
15–19[a]	3.01	n.i.	3.10
16–20[a]	2.95	3.13	3.18
17–21	2.90	3.84	3.18
18–22	2.93	2.85	3.04
19–23[a]	3.06	3.48	3.53
20–24	2.78	2.79	2.88
21–25	2.98	3.00	3.09
22–26[a]	3.19	3.25	3.32
23–27[a]	3.03	2.80	3.01
24–28	2.87	2.86	3.04
25–29	2.02	2.77	3.27
26–30[a]	3.06	3.07	3.32
27–31	2.97	2.90	2.96
mean distance	2.97	3.04	3.15
mean d-H-a angle	160°	164°	169°

[a] hydrophilic environment n.i. not identified

Table 6. Average rms fluctuation of certain atoms derived from 5–15 ps of the MDC and MDS simulations as well as from the *B*-values of the X-ray structure

Average over atoms	$(3B/8\pi^2)^{1/2}$ [Å]	$\langle(\Delta r)^2\rangle^{1/2}$ [Å]	
		$\text{MDC}_{5-15\text{ ps}}$	$\text{MDS}_{5-15\text{ ps}}$
all	0.71	0.72	0.75
C_α	0.62	0.48	0.53
C_β	0.67	0.57	0.62
C_γ	0.77	0.64	0.73
C_δ	0.82	0.75	0.79
C_{ε_1}	0.74	0.92	1.05

there are longer as well as shorter H-bonds than in the X-ray structure though their average length is slightly greater. In $\overline{\text{MDS}}$ on the other hand H-bonds are consistently longer. This is in accordance with the picture suggested by the dihedral angles. A small part of the bond energy lost due to increased donor-acceptor distances seems to be recovered by more favourable hydrogen bond angles (see Table 5). The "untightening" of the helix in the course of the MDS simulation may also in part be responsible for the 6.3% lower number density of $\overline{\text{MDS}}$ as compared to the X-ray structure (3.6% lower in $\overline{\text{MDC}}$).

Flexibility and dynamics

The mobility of atoms is given in terms of their rms fluctuations $\langle\Delta r^2\rangle^{1/2}$ which are closely related with crystallographic *B*-values $\langle\Delta r^2\rangle = 3B/8\pi^2$. Comparison of rms fluctuations and *B*-values suffers from two shortcomings: *B*-values are also subsuming contributions from static disorder in the crystal, and rms fluctuations obtained for a longer time span of MD simulation cannot distinguish motions about a stable centre of mass from motions of the mass centre itself. Average rms fluctuations calculated from the *B*-values of the X-ray structure and from 5 to 15 ps of the MDC and the MDS simulation are listed in Table 6. As expected the values consistently increase with increasing distance of the carbon atoms from the main chain. Possibly due to static disorder effects, the values derived from the temperature factors are higher than those from the MDC and, to a lesser extent, from the MDS simulation.

The average fluctuations of the main-chain atoms and of the side-chain atoms per residue are plotted as histograms in Fig. 10. The overall correlation coefficients between the rms fluctuations from the simulations and the *B*-values are $r_{\text{MDC}} = 0.53$ and $r_{\text{MDS}} = 0.40$ for the main-chain, and $r_{\text{MDC}} = 0.26$ and $r_{\text{MDS}} = 0.01$ for the side-chain atoms. The extremely high *B*-values for the main chain at the *C*-terminus do not find an outstanding correspondence in the simulated fluctuations which, though clearly above those of the preceding α-helix, in the MDS simulation are surpassed by the bend residues. In view of the side-chain fluctuations, however, one hesitates to conclude that the high *C*-terminal *B*-values were due to static disorder rather than to conformational flexibility. Figure 11 (see colour page) shows the distribution of different degrees of mobility over the aPP molecule. The atoms are classified in 4 appropriate groups according to their individual rms fluctuations and are represented by means of a colour code.

The largest differences between MDS and *B*-derived fluctuations are found for the side chains of Asp 11 (+0.71 Å), Glu 15 (+0.72 Å), Arg 19 (−0.38 Å), Phe 20 (+0.61 Å), and Arg 33 (+0.62 Å). As correspondingly high positional differences are found for the polar side chains 11, 15, 19, and 33 their fluctuations should comprise displacement of their mass centres. One would tend to predict drastic differences for side chains which are exposed upon dissociation of the dimer. Tyr 7 and Tyr 21, however, the most prominent intermonomer contacts, have surprisingly small differences (−0.23 and −0.11 Å respectively). This is in line with the findings on the differences in position and accessible surface for these residues described above.

On the other hand there is one side chain, that of Phe 20, which is found amongst those with the largest differences in rms fluctuations although it is part of the hydrophobic core and not sticking out

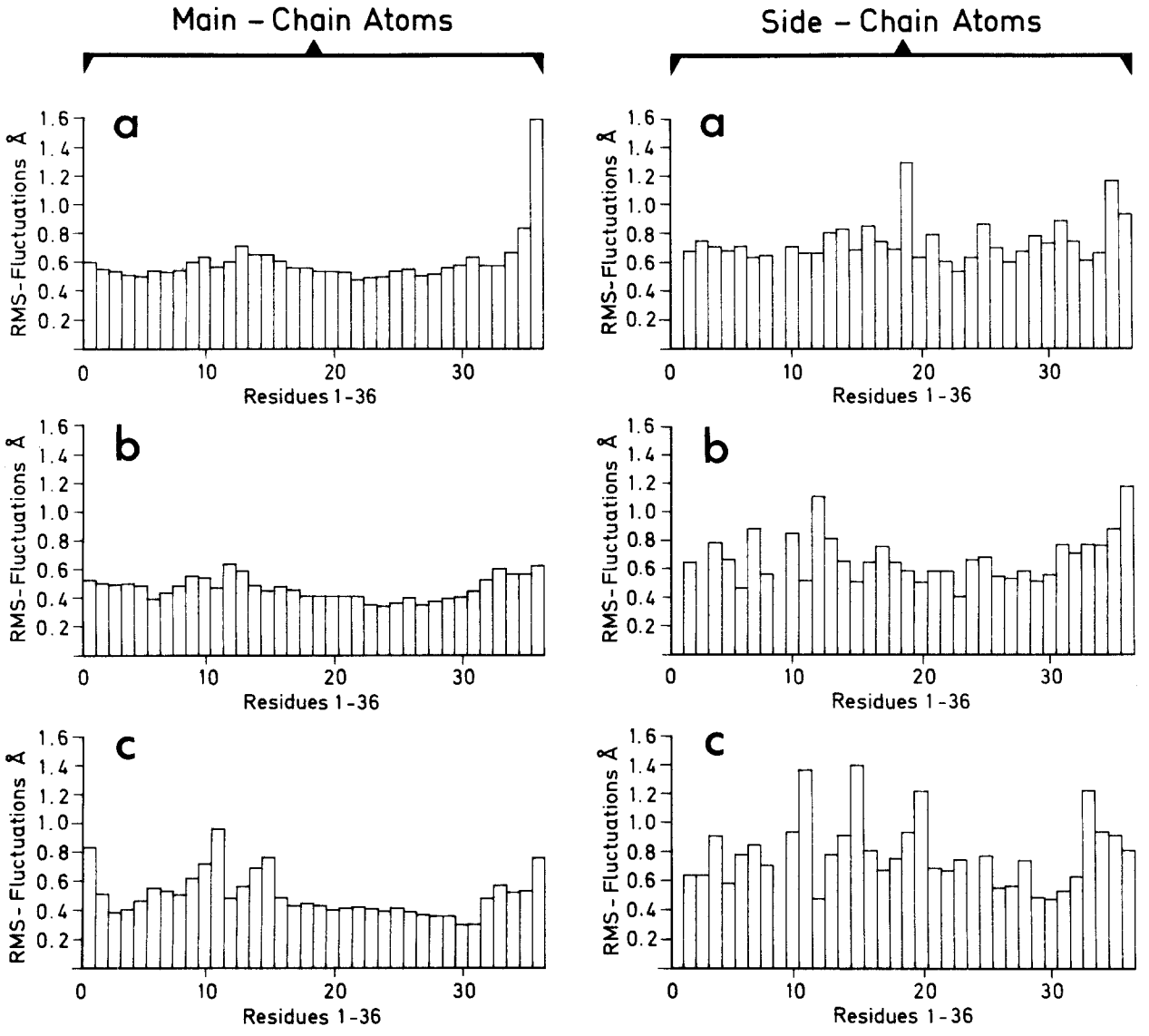

Fig. 10. Rms fluctuations of main-chain atoms (*left*) and side-chain atoms (*right*). **a** derived from the *B*-values of the X-ray structure; **b** calculated over 5–15 ps of the MDC simulation; **c** calculated over 5–15 ps of the MDS simulation

into the solvent like Asp 11, Glu 15, Arg 19 and Arg 33. This finding suggested a more detailed analysis of Phe 20 with respect to other parameters. The χ^1 and χ^2 dihedral angles of the Phe 20 side chain as a function of simulation time are depicted in Fig. 12. After 7 ps, χ^1 undergoes an abrupt transition from about 160 to 80° which only takes 0.3 ps. Several phases of the transition are shown in Fig. 13 (see colour page). The event is perceived also by χ^2 which, after two larger opposite deflections, continues oscillating about the same average value. The behaviour of χ^1 is unique among all side chains which are part of the core. Since Phe 20 is the only phenylalanine in aPP the alteration of its microenvironment upon dissociation of the dimer seems particularly suitable for being probed by NMR spectroscopy. It appears possible that the switch in the orientation of Phe 20 is temporally and spatially related to the motion undergone by the turn region (see Figs. 3 b and 14). The conformational change of the turn produced in the MDS simulation is reflected in the average rms fluctuation of the side-chain atoms of residues 9–12, which is 0.92 as compared to 0.83 for the MDC simulation and deviates more from the *B*-derived value than the latter.

4. Summary

In summary the MD simulations of aPP in solution and in the crystal and the comparison of the respective mean structures with one another and with the X-ray structure reveal the following features:

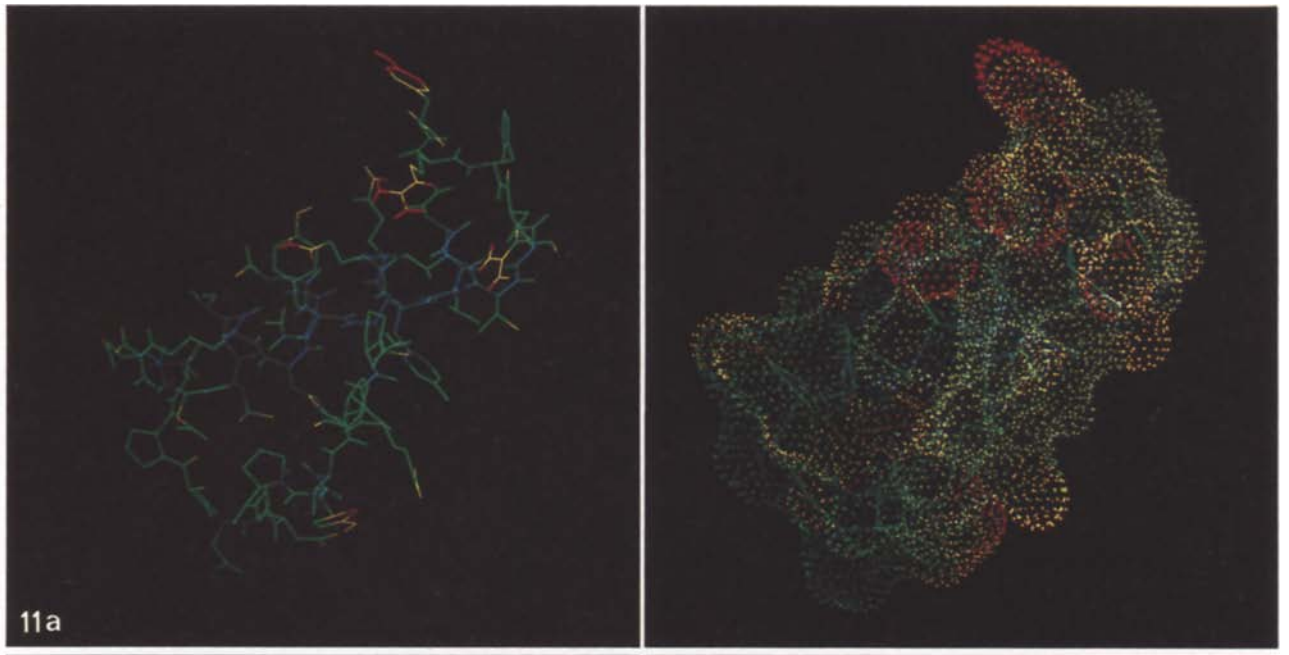

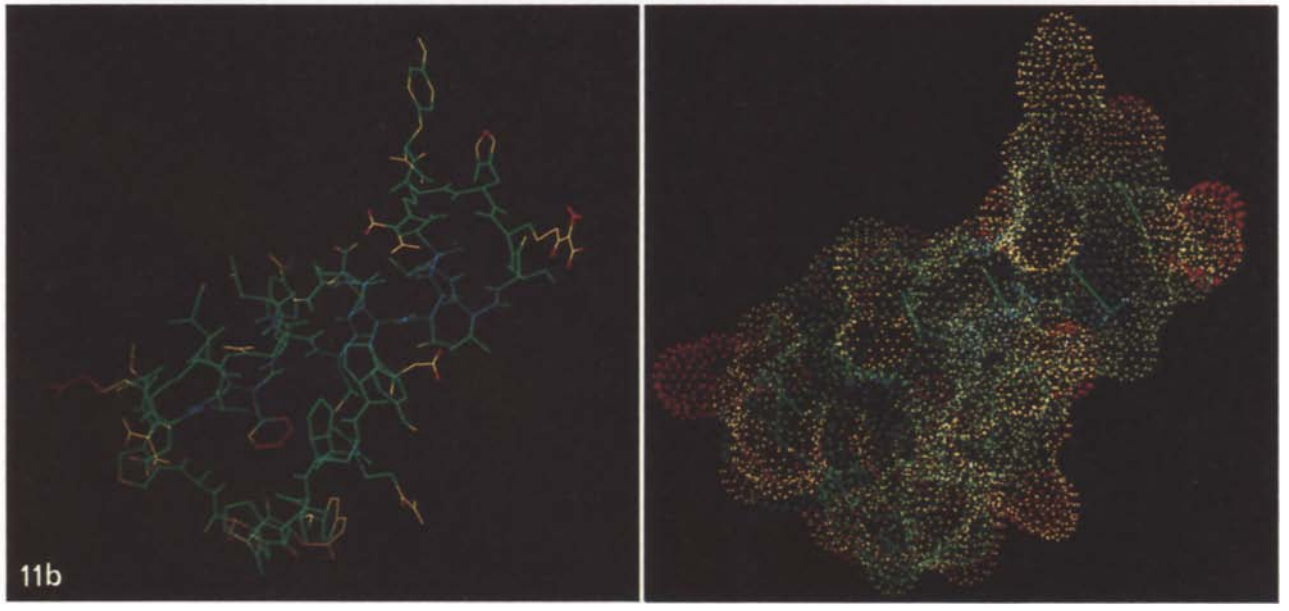

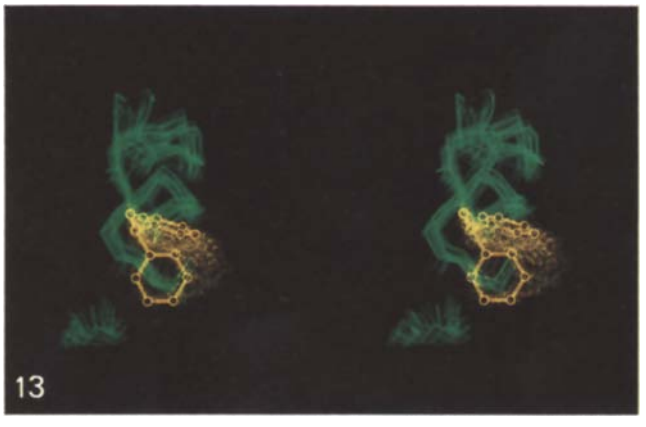

Fig. 11. Distribution of different degrees of mobility over the aPP molecule in the bond skeleton and in the dotted surface (Conolly 1983) representation. **a** $\overline{\text{MDC}}$; **b** $\overline{\text{MDS}}$. Classification of atoms according to their rms fluctuations (5–15 ps) and corresponding colour code:

0 – 0.4 Å: blue
0.4 – 0.8 Å: green
0.8 – 1.2 Å: yellow
> 1.2 Å: red

Fig. 13. Stereo tracing of the change in orientation of the Phe 20 side chain (yellow). (States before and after the transitions are set off against transient phases.)

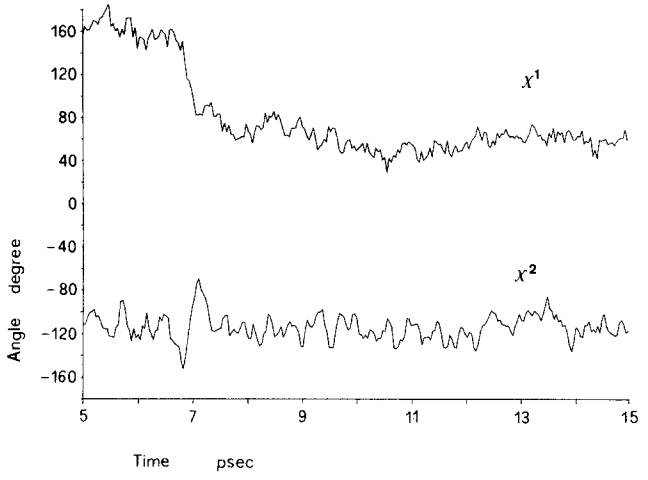

Fig. 12. Side-chain dihedral angles χ^1 and χ^2 of Phe 20 as a function of simulation time

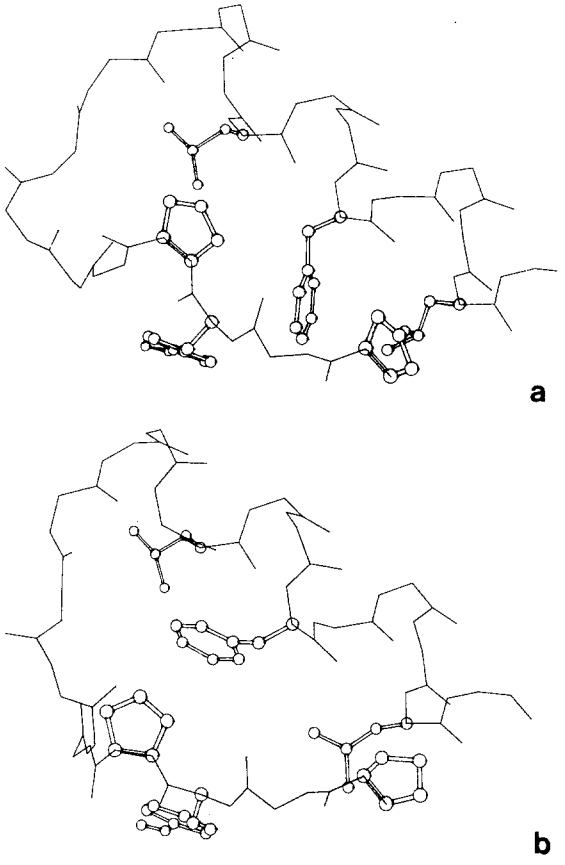

Fig. 14. The turn region of aPP **(a)** before and **(b)** after its displacement in the MDS simulation (5 and 15 ps). See differences in turn width and orientation of Phe 20

In the MDC simulation the system is equilibrated after a relatively short time and deviations from the X-ray structure remain within narrow limits. In the simulation for the monomer in solution, MDS, the β-bend and adjacent residues of the polyproline helix are excepted from the overall equilibration: After 9 ps they start moving away from the X-ray structure – the bend widens – an occurrence primarily reflected in larger positional differences and rms fluctuations. In the crystal this part of the molecule seems to be stabilized by the force field of the surrounding molecules.

Residues which in the dimer are shielded from water contact are less affected than anticipated when solvent-exposed at the surface of the isolated monomer. Tyr 7 and Tyr 21 at least, the most prominent dimer-forming side-chains, do not tend to avoid the contact with water. A side chain of the hydrophobic core, Phe 20 on the other hand, imposes large rms fluctuations in the MDS simulation, otherwise encountered only with the atoms of exposed polar side chains like Asp 11, Glu 15, Arg 19, and Arg 33. The time dependence of the χ^1 dihedral angle of Phe 20 reveals an abrupt reorientation which may be temporally and spatially related to the motion of the β-turn region. The fact that Phe 20 is the only phenylalanine in aPP suggests that the alteration of its microenvironment upon dissociation of the dimer could be demonstrated by NMR spectroscopy. The outstanding flexibility in the main-chain *C*-terminus as derived from the *B*-values of the X-ray structure is much less pronounced in both the MDC and MDS simulation.

A more detailed analysis of the α-helix shows that the main-chain dihedral angles are shifted from values generally encountered in crystal structures towards those of the ideal Pauling helix. There is concomitant elongation of H-bonds. Though present also in the MDC simulation as a tendency these effects are pronounced and consistent in the MDS simulation.

Acknowledgements. We wish to thank Prof. T. L. Blundell, FRS, of Birkbeck College, London, and his coworkers, in particular J. P. Pitts, J. D. Glover, and I. Haneef for providing the atomic coordinates of aPP and for continued cooperation on pancreatic polypeptide hormones. Valuable discussions with Prof. Fleischhauer, Lehr- und Forschungsgebiet Theoretische Chemie, RWTH Aachen, are highly appreciated. Thanks are due to the Abteilung Medizinische Statistik und Dokumentation, RWTH Aachen, for access to the VAX 11/780 computer and to the Rechenzentrum der RWTH Aachen for providing colour microfilm facilities. This work was supported by grants from the Deutsche Forschungsgemeinschaft and the Fonds der Chemischen Industrie.

References

Berendsen HJC, Postma JPM, van Gunsteren WF, Hermans J (1981) Interaction models for water in relation to protein hydration. In: Pullman B (ed) Intermolecular forces. Reidel, Dordrecht, pp 331–342

Berendsen HJC, Postma JPM, van Gunsteren WF, DiNola A, Haak JR (1984) Molecular dynamics with coupling to an external bath. J Chem Phys 81:3684–3690

Blundell TL, Pitts JE, Tickle IJ, Wood SP, Wu CW (1981) X-ray analysis (1.4-Å resolution) of avian pancreatic polypeptide: Small globular protein hormone. Proc Natl Acad Sci USA 78:4175–4179

Blundell TL, Barlow D, Borkakoti N, Thornton J (1983) Solvent-induced distortions and the curvature of α-helices. Nature 306:281–283

Glover I, Haneef I, Pitts J, Wood S, Moss D, Tickle I, Blundell T (1983) Conformational flexibility in a small globular hormone: X-ray analysis of avian pancreatic polypeptide at 0.98-Å resolution. Biopolymers 22:293–304

Glover ID, Barlow DJ, Pitts JE, Wood SP, Tickle IJ, Blundell TL, Tatemoto K, Kimmel JR, Wollmer A, Straßburger W, Zhang YS (1984) Conformational studies on the pancreatic polypeptide hormone family. Eur J Biochem 142:379–385

Hermans J, Berendsen HJC, van Gunsteren WF, Postma JPM (1984) A consistent empirical potential for water-protein interactions. Biopolymers 23:1513–1518

Lee B, Richards FM (1971) The interpretation of protein structures: Estimation of static accessibility. J Mol Biol 55:379–400

Pearlman RS (1981) SAREA: Van der Waals (and accessible) surface area of molecules. QCPE Bull 1:16

van Gunsteren WF, Berendsen HJC (1977) Algorithms for macromolecular dynamics and constrained dynamics. Mol Phys 34:1311–1327

van Gunsteren WF, Berendsen HJC (1982) Molecular dynamics: perspective for complex systems. Biochem Soc Trans 10:301–305

van Gunsteren WF, Berendsen HJC (1984) Computer simulation as a tool for tracing the conformational differences between proteins in solution and in the crystalline state. J Mol Biol 176:559–564

van Gunsteren WF, Karplus M (1982) Protein dynamics in solution and in a crystalline environment: A molecular dynamics study. Biochemistry 21:2259–2274

van Gunsteren WF, Berendsen HJC, Hermans J, Hol WGJ, Postma JPM (1983) Computer simulation of the dynamics of hydrated protein crystals and its comparison with X-ray data. Proc Natl Acad Sci USA 80:4315–4319

Conolly ML (1983) Solvent-accessible surfaces of proteins and nucleic acids. Science 221:709–713